JOURNAL OF GEOPHYSICAL RESEARCH, VOL. 111, G02016, doi:10.1029/2005JG000142, 2006

Global distribution and seasonality of active fires as observed with the Terra and Aqua Moderate Resolution Imaging Spectroradiometer (MODIS) sensors

Louis Giglio,[1,2] Ivan Csiszar,[2] and Christopher O. Justice[2]

Received 22 November 2005; revised 28 February 2006; accepted 9 March 2006; published 10 June 2006.

[1] We describe a new global multiyear satellite fire product designed to meet the needs of the global modeling community. We use the new data set to analyze the global distribution of biomass burning using five different temporal metrics derived from 5 years of high-quality satellite data acquired with the Moderate Resolution Imaging Spectroradiometer (MODIS), on board NASA's Terra satellite. The global distributions of fire pixel density, peak month, season length, and annual periodicity are described. As part of our analysis we show, for the first time, the global distribution of the fire radiative power (FRP), a relatively new remotely sensed quantity. We find that low FRP tends to be associated with areas of cropland burning. In the tropics and much of the subtropics, low FRP is also associated with more heavily forested areas, while higher FRP tends to occur in areas of grassland burning. In boreal forests this trend is reversed, with higher FRP occurring in areas of greater tree cover. We next combine 3 years of Terra and Aqua MODIS observations to show that a strong diurnal fire cycle is prevalent at tropical and subtropical latitudes. We also consider the consistency of the fire time series recorded by the two MODIS instruments, and find the month of peak burning and fire season length observed by each to be in good agreement in most areas. However, significant discrepancies with respect to seasonality do occur in some relatively small areas, and are most pronounced in tropical rain forest.

Citation: Giglio, L., I. Csiszar, and C. O. Justice (2006), Global distribution and seasonality of active fires as observed with the Terra and Aqua Moderate Resolution Imaging Spectroradiometer (MODIS) sensors, *J. Geophys. Res.*, *111*, G02016, doi:10.1029/2005JG000142.

1. Introduction

[2] Biomass burning associated with human land-use activities, as well as naturally occurring wildfire, has come to be recognized as having an important role in regional and global climate change [*Andreae*, 1991]. More recently, biomass burning has been found to affect weather on much shorter timescales [*Rosenfeld*, 1999] and has even been implicated in the death of coral reefs [*Abram et al.*, 2003]. With a more variable and changing climate, fire distributions and regimes are likely to change [*Kasischke et al.*, 1995; *Weber and Flannigan*, 1997]. There is consequently a considerable need for long-term global fire information. At present the only practical way to monitor fire activity at a continental or global scale is with sensors on terrestrial satellites [*Justice and Korontzi*, 2001].

[3] The launch of NASA's Terra satellite in late 1999 marked a significant step forward in the ability to monitor fires from space. The satellite's sensor payload includes the Moderate Resolution Imaging Spectroradiometer (MODIS), an instrument having 1-km middle- and long-wave infrared bands designed specifically for the observation of actively burning fires [*Kaufman et al.*, 1998]. In addition to offering enhanced fire detection, these bands permit, for example, low-intensity surface fires to be distinguished from higher-intensity crown forest fires [*Kaufman et al.*, 2003; *Wooster and Zhang*, 2004]. The Terra satellite occupies a sun-synchronous polar orbit with local equatorial crossing times of 1030 (descending) and 2230 (ascending). A second MODIS instrument on NASA's Aqua satellite, launched in mid-2002, provides an additional pair of observations at 0130 (descending) and 1330 (ascending) local time.

[4] After nearly 6 years of data collection, there is now a sufficiently long observational record to begin meaningful time series analyses of fire activity with MODIS data. While some longer time series fire data sets produced with other satellite sensors are available, their application to the study of global fire activity is more limited for various reasons. The combined Along Track Scanning Radiometer (ATSR) and Advanced Along Track Scanning Radiometer (AATSR) World Fire Atlas [*Arino and Rosaz*, 1999], for example, currently available from July 1996 through the present, is composed exclusively of nighttime fire observations; this can skew the apparent distribution of fire activity in those regions having a strong diurnal fire cycle. The Tropical Rainfall Measuring Mission (TRMM) Visible and Infrared

[1] Science Systems & Applications, Inc., Lanham, Maryland, USA.
[2] Department of Geography, University of Maryland at College Park, College Park, Maryland, USA.

0148-0227/06/2005JG000142

Scanner (VIRS) monthly fire product [*Giglio et al.*, 2003a], which currently spans January 1998 through the present, is restricted to tropical and subtropical latitudes by the highly inclined orbit of the TRMM satellite. Although fire data sets are routinely generated for some regions using NOAA Advanced Very High Resolution Radiometer (AVHRR) 1-km data, global data sets are only available for a limited period [*Stroppiana et al.*, 2000]. A further limitation common to these data sets arises from the fact that the sensors from which they were derived were not intended for monitoring fires. As such, their optical and radiometric specifications, most importantly the levels at which the bands useful for fire monitoring saturate, generally preclude fire characterization beyond simply flagging the existence of one or more active fires within a pixel.

[5] In this paper, we examine global fire activity using observations made with the MODIS instruments on board NASA's Terra and Aqua satellites. As part of our analysis we present, for the first time, a global picture of the middle-infrared fire radiative power (FRP), a relatively new remotely sensed quantity proposed by *Kaufman et al.* [1998]. Our work complements earlier global fire studies based solely on fire count information by *Dwyer et al.* [1999, 2000a] using the AVHRR Global Fire Product [*Stroppiana et al.*, 2000] from April 1992 through March 1993, and by *Csiszar et al.* [2005], who used the first 2 years of MODIS fire observations. In section 2 we describe the remotely sensed data used in this study, and include a detailed description of the new MODIS Climate Modeling Grid (CMG) active fire products. These summary products are generated from the full resolution, orbital data to facilitate global analyses. Next, in section 3, we describe the spatial and temporal metrics used to extract summary information from the time series of MODIS fire observations. In section 4 we use the metrics to examine the global distribution of biomass burning, and perform a preliminary examination of the diurnal fire cycle using combined Terra and Aqua MODIS observations. In section 5, we quantify the extent to which the Terra and Aqua MODIS fire data records are in agreement with respect to the seasonality of fire activity. Finally, in section 6, we examine the sensitivity of our results to seasonal and interannual variations in cloud cover.

2. Data

2.1. MODIS Climate Modeling Grid (CMG) Fire Products

[6] The MODIS Climate Modeling Grid (CMG) fire products have recently been developed and are primarily intended to facilitate the incorporation of the MODIS active fire data into global emissions and chemical transport models [*Justice et al.*, 2002]. Recent applications include work by *Edwards et al.* [2004, 2005] and *Giglio et al.* [2006]. Currently, the Terra and Aqua CMG fire products are generated on a monthly basis at 0.5° spatial resolution to maintain compatibility with the AVHRR Global Fire Product, and an earlier multiyear fire data set derived from TRMM VIRS data [*Giglio et al.*, 2003a]. Higher spatial and temporal resolution MODIS CMG fire products (8 days, 0.25°) are presently being generated on an experimental basis. In this study we used the Collection 4 Terra and Aqua MODIS monthly CMG fire product at 0.5° spatial resolution ("MOD14CMH" and "MYD14CMH"), from November 2000 (Terra) and July 2002 (Aqua) through October 2005. Here we briefly describe the individual data layers of the current CMG fire product suite.

2.1.1. Overpass-Corrected Fire Pixel Counts

[7] As discussed by *Giglio et al.* [2003a], the traditional "gridded fire counts" obtained from polar orbiting satellites are biased at high latitudes owing to nonuniform spatial and temporal sampling. The total number of fire pixels observed in each grid cell is therefore corrected for multiple satellite overpasses and missing observations. This is accomplished by normalizing the raw fire pixel counts by the expected equatorial coverage in a complete calendar month containing no missing observations. The overpass-corrected fire pixel count in the grid cell located at row i and column j, denoted as $N'_{\text{fire}}(i, j, t)$, is given by

$$N'_{\text{fire}}(i,j,t) = \frac{N_{\text{fire}}(i,j,t) N_{\text{days}}(t) A(i) N_{\text{eq}}}{N_{\text{total}}(i,j,t) A_{\text{eq}}}, \quad (1)$$

where $N_{\text{fire}}(i, j, t)$ is the number of active fire pixels detected in the grid cell over a given calendar month indexed by t, $N_{\text{total}}(i, j, t)$ is the total number of MODIS pixels that fell within the grid cell during the calendar month, $N_{\text{days}}(t)$ is the number of days in the calendar month, $A(i)$ is the area of the grid cell (solely a function of i due to the equal-angle grid used to composite pixels), A_{eq} is the area of a grid cell along the equator, and N_{eq} is the expected number of MODIS pixels within a grid cell located along the equator during a full 24-hour day of no missing observations. The value of this last constant was determined empirically using 1 year of observations from 2001.

2.1.2. Mean Cloud Fraction

[8] The average fraction of each grid cell obscured by cloud during a given calendar month, $\bar{f}_{\text{cloud}}(i, j, t)$, defined as

$$\bar{f}_{\text{cloud}}(i,j,t) = \frac{N_{\text{cloud}}(i,j,t)}{N_{\text{total}}(i,j,t)}, \quad (2)$$

where $N_{\text{cloud}}(i, j, t)$ is the total number of cloud pixels within the grid cell during calendar month t.

2.1.3. Cloud-and-Overpass-Corrected Fire Pixels

[9] The number of fire pixels observed in each grid cell, corrected for multiple satellite overpasses, missing observations, and variable cloud cover. The cloud-and-overpass-corrected fire pixel count, denoted as $N''_{\text{fire}}(i, j, t)$, is given by

$$N''_{\text{fire}}(i,j,t) = \frac{N'_{\text{fire}}(i,j,t)}{1 - \bar{f}_{\text{cloud}}(i,j,t)}. \quad (3)$$

Grid cells for which the mean cloud fraction is 1 are assigned a cloud-and-overpass-corrected fire pixel count of zero. This correction is based upon the assumption that the number of fire pixels per unit area within both clear and cloud-obscured areas is identical, an assumption which is not always reasonable [*Eva and Lambin*, 1998]. In the future we will incorporate a more realistic cloud correction that distinguishes between raining and non-raining clouds. Figure 1 illustrates the effects of the overpass-correction and

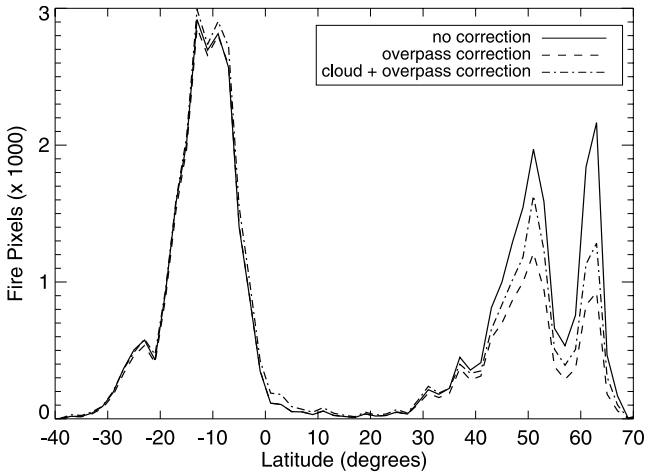

Figure 1. Zonal profile of fire-pixel counts from the July 2002 Terra CMG product illustrating the typical effect of the overpass and cloud-and-overpass corrections (dashed lines) on the uncorrected (raw) fire-pixel counts (solid line).

the cloud-and-overpass-correction for the July 2002 Terra CMG product.

2.1.4. Mean Fire Radiative Power

[10] The mean fire radiative power (FRP) of all fire pixels in each grid cell during a calendar month. The FRP retrieval [*Kaufman et al.*, 1998] requires an estimate of the background, middle infrared nonfire radiance (or brightness temperature) in the immediate vicinity of the fire. This quantity, which is computed as part of the background characterization phase of the fire detection algorithm [*Giglio et al.*, 2003b], is sometimes unavailable in the neighborhood of heavy cloud cover, very large fires, and small islands or peninsulas. Fire pixels for which this is the case are not included in the calculation of the mean. Fire pixels detected at scan angles above 40° are also excluded as they are affected by a significant off-nadir bias.

[11] The utility of the FRP for estimating combusted biomass was first proposed by *Kaufman et al.* [1998] and subsequently refined by *Wooster et al.* [2003]. In short, the remotely sensed FRP is, to a good approximation, equivalent to the total radiative power of the fire as described by the Stefan-Boltzmann law. By integrating the FRP over the duration of a fire, one obtains the fire radiative energy (FRE). To the extent this latter quantity is proportional to the total energy released during combustion, one can calculate the mass of fuel consumed given the heat of combustion for that fuel. For vegetation there is fortunately relatively little variation in the latter quantity, and a constant value can usually be assumed everywhere [*Johnson*, 1992]. Although the original goal in developing the FRP was to improve estimates of pyrogenic emissions, the mean FRP can also provide useful information about fire behavior. This will be discussed in section 4.3.

2.1.5. Land Cover Statistics

[12] For emissions modeling, land cover information is often used to determine fuel loads and emission factors [e.g., *Streets et al.*, 2003]. Within the CMG product we have therefore included the mean percent tree cover, percent herbaceous vegetation cover, and percent bare ground from the global MODIS Vegetation Continuous Fields (VCF) products [*Hansen et al.*, 2003] for all fire pixels within each grid cell during a given calendar month.

2.1.6. Mean Detection Confidence

[13] The mean detection confidence of all fire pixels detected within each grid cell, included primarily for quality assurance. The detection confidence, which varies between 0 and 100%, is a heuristic measure of the radiometric contrast between a fire pixel and its immediate non-fire neighborhood, with extra penalties imposed near potential false alarm sources such as cloud edges and coastline [*Giglio et al.*, 2003b].

2.1.7. Additional Data Layers

[14] Additional layers containing simple counts of missing data, unknown and total pixels are included to assist quality assurance and simplify the production of experimental high-level data sets.

[15] In generating the above data layers, fire pixels associated with persistent static fire sources were excluded. These were identified on a 1-km global grid as follows: any 1-km grid cell in which fire pixels were detected on 50 or more unique calendar days per year was deemed a persistent source not representing a vegetation fire. The majority represent static gas flares associated with oil drilling. Though small in size, gas flares usually burn at comparatively high temperatures, typically between 1000 K and 1900 K [*Scottish Environment Protection Agency*, 2002], and are readily detected by satellite sensors. They have been mapped extensively by *Elvidge et al.* [1997] using the Defense Meteorological Satellite Program Operational Linescan System, and occur primarily in North Africa, the Middle East, Gabon, Russia, and Ukraine. Persistent fire pixels are also associated with active volcanoes and a smaller number of unknown sources (possibly power stations) located within urban areas. Sources in this last category may represent recurring false alarms near industrial sites and are being investigated as part of our ongoing validation activities.

2.2. Agricultural Data

[16] We used the *Ramankutty and Foley* [1998] version 1.1 global croplands data set, at 0.5° spatial resolution, to supply agricultural land-use distributions.

3. Analysis Approach

[17] Our analysis is similar to that used by *Dwyer et al.* [1999, 2000a] with the 21-month AVHRR Global Fire Product [*Stroppiana et al.*, 2000]. We generated a "climatological" Terra MODIS monthly data set by independently averaging the overpass-corrected fire pixel counts for each calendar month from November 2000 through October 2005. We then extracted multiple spatial and temporal metrics from this climatological data set, as well as the full monthly Terra time series. Within these metrics we next identified patterns and trends, which we interpreted with respect to different biophysical variables and current knowledge of regional burning practices. Our goal was to describe and, in part, explain the global spatial and temporal distribution of fire activity as observed by MODIS.

3.1. Spatial Metrics

[18] We calculated the average annual overpass-corrected fire pixel density for MODIS by summing the average monthly overpass-corrected fire counts and dividing by grid cell area. The latter step was necessary to compensate for the non-equal area of the equal-angle grid cells used to bin the data. We also averaged the November 2000 to October 2005 Terra MODIS monthly fire radiative power (FRP), weighted by the number of overpass-corrected fire pixels for each month, to produce a climatological map of mean annual FRP. Grid cells containing fewer than five fire pixels per year were deemed as having little real signal and were excluded from the subsequent analysis.

3.2. Spatiotemporal Metrics

[19] Global fire activity exhibits a strong seasonality that can be characterized using any number of parameters in both the time and frequency domain. Here we have selected three different temporal metrics, computed independently for each grid cell, that are intuitive and readily understood. First, we define the peak in fire activity as the calendar month during which the maximum number of average monthly overpass-corrected fire counts was detected. Second, we define the duration of the fire season as the number of months during which the average monthly overpass-corrected fire counts was at least 10% of the average annual overpass-corrected fire counts. Third, we employ the 12-month lagged autocorrelation of the full 5-year monthly time series to provide a measure of the interannual variability and periodicity of fire activity. Grid cells having very similar annual cycles of fire activity will have a 12-month lagged autocorrelation approaching +1, while those grid cells exhibiting significant interannual variability have positive or negative values much closer to zero. (An autocorrelation approaching −1 would indicate a significant biannual fire cycle. This might happen as a result of specific agricultural practices, but is otherwise not expected.) We expect the 12-month lagged autocorrelation to provide a combined measure of anthropogenic (versus natural) fire activity and climatic constraints. Specifically, regions of high anthropogenic fire activity and low interannual rainfall variability should exhibit a very high temporal autocorrelation. Conversely, regions of low anthropogenic fire activity and high interannual rainfall variability should exhibit a very low temporal autocorrelation. The remaining cases, high anthropogenic fire activity/high rainfall variability and low anthropogenic fire activity/low rainfall variability, should exhibit moderately high and moderately low temporal autocorrelation, respectively.

4. Results

4.1. Fire Counts

[20] The average annual overpass-corrected fire pixel density for the Terra MODIS is shown in Figure 2a. The overall pattern is largely consistent with that found by *Dwyer et al.* [2000b] using 1 year of the AVHRR Global Fire Product (GFP). There are some substantial differences, however, in the distribution of areas containing little or no fire activity. With respect to those areas in which the MODIS fire product shows significant fire activity while the GFP shows none, this is explained by the static desert mask used in the production of the AVHRR data set. This mask was used to identify, a priori, those regions in which fires should not occur and thereby remove false detections over hot desert surfaces that are problematic for the GFP algorithm [*Stroppiana et al.*, 2000]. Within some of these regions, however, fires do in fact occur, most notably in northwest Australia. Possible explanations for the complimentary case in which the GFP shows significant fire activity in locations where the MODIS fire product shows little or no fire activity are most likely due to interannual variability and a much higher incidence of false detections in the GFP [*Giglio et al.*, 1999; *Ichoku et al.*, 2003; *Csiszar et al.*, 2005]. With respect to the latter point, the GFP shows widespread burning across the entire continental United States, for example, which does not actually occur.

[21] The location of greatest annual fire activity occurs within the so-called Arc of Deforestation in Brazil at approximately 13°S, 55°W. Barring static gas flares, the density of fire pixels detected at this location is more than a factor of two higher than anywhere else in the world. This is a region of intense land-cover conversion in which rain forest is rapidly being transformed into pasture, with subsequent burning of the forest slash and repeated burning for pasture maintenance.

4.2. Seasonality

[22] The peak month of Terra MODIS fire activity is shown in Figure 2b. At the global scale, July, August, and September are the peak months of fire occurrence, with fires in both the Northern and Southern Hemispheres, while February is least often the month of peak fire occurrence. The most striking feature is perhaps the six-month difference in the timing of greatest fire activity in Africa north and south of the Equator, as a consequence of the opposite phase in the timing of the African dry season in these regions. Global patterns in the seasonality of fire counts have previously been described by *Dwyer et al.* [1999, 2000b], *van der Werf et al.* [2003], and *Csiszar et al.* [2005], and will not be repeated here, but it is worth reiterating that both the peak month and the duration of the fire season are coupled to the seasonal cycle of precipitation, particularly in the tropics. (Note that *Dwyer et al.* [1999, 2000b] used a somewhat different criterion for identifying the "central time" of fire activity, namely the calendar month during which 50% of the cumulative monthly fire pixels from April 1992 through March 1993 were detected.)

[23] Fire season duration is shown in Figure 2c. Globally, the duration of the annual fire season usually varies between 2 and 6 months and is, in the tropics, highly constrained by the duration of the dry season. Exceptionally long fire seasons of ∼10 months occur in central and southern Brazil and the southeastern United States. A similarly long fire season occurs in a small area in eastern Australia (approximately 28°S, 149°E) and might be associated with sugarcane residue burning that takes place throughout the comparatively long (∼8 month) harvesting season. An analysis at higher spatial resolution is ultimately needed to verify this hypothesis. The duration of the fire season at boreal latitudes is uniformly short at 1–3 months, and is constrained by the seasonality of circulation patterns [*Johnson*, 1992].

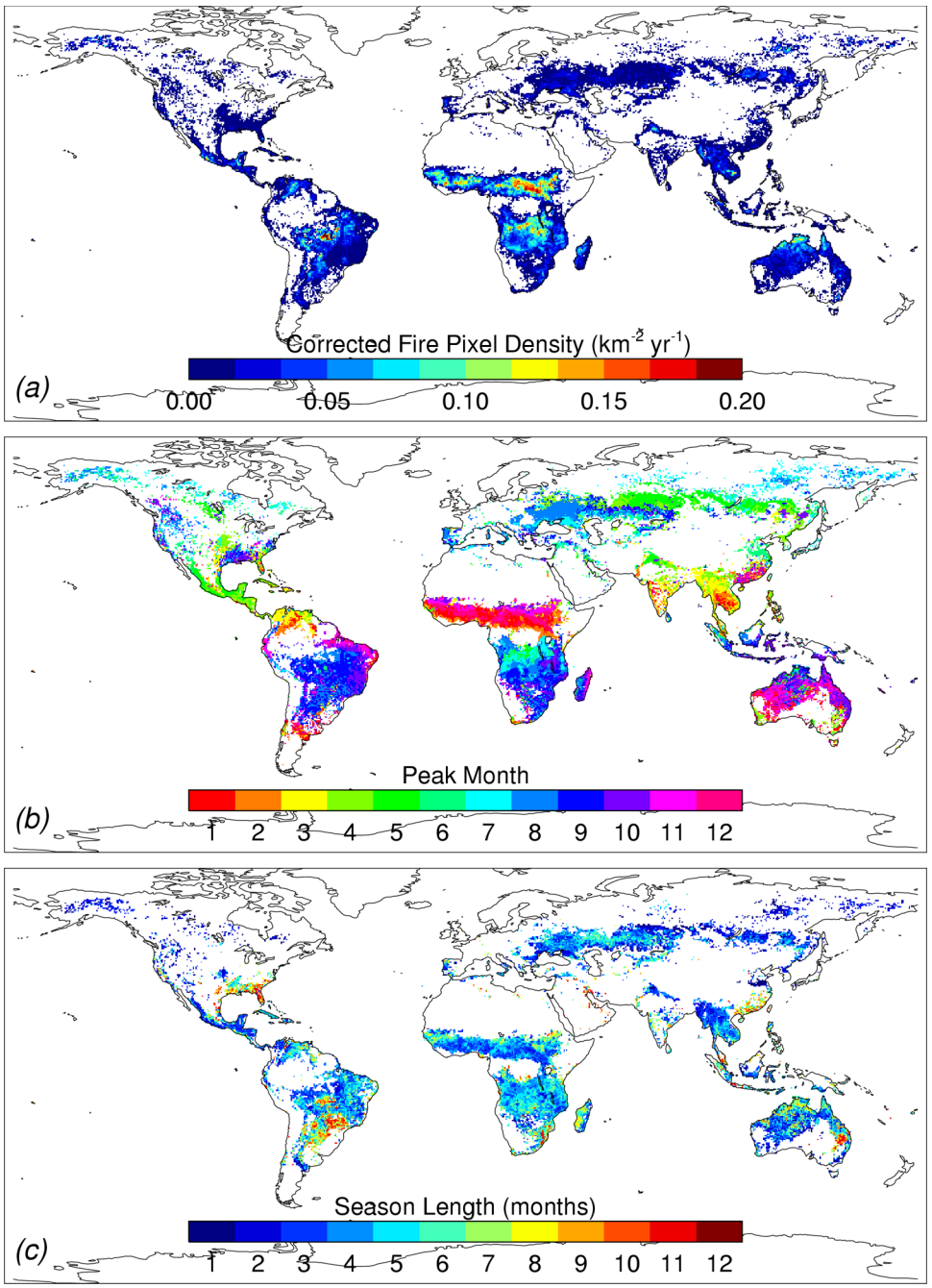

Figure 2. Climatological fields derived from the first 5 years of Terra MODIS fire observations (November 2000 to October 2005). (a) Mean annual overpass-corrected fire pixel density, (b) month of maximum climatological fire activity, and (c) fire season length.

[24] The highest 12-month lagged temporal autocorrelation (Figure 3a) occurs in the savannas of Africa, both in the Sudanian and Sahelian zones north of the equator and in central and southern Africa between 5°S and 20°S, reflecting the extremely periodic seasonal cycle of fire activity in these regions, and also indicating that they experience less interannual variability. This characteristically strong annual periodicity is caused by a combination of widespread human-induced burning for land maintenance purposes and low interannual variability in rainfall during the study period. The areas to the north and south of these two regions, respectively, show decreasing annual autocorrelation associated with greater interannual variability in rainfall and grass (fuel) production. Other regions of very high temporal autocorrelation occur in the tropics, for example, Thailand, Cambodia and Laos in Southeast Asia, Mexico and Central America, and the Llanos, Mato Grosso, and Brazilian Highlands of South America. The small spot of high periodicity in northern India (31°S, 75°E) reflects seasonal agricultural waste burning at the beginning and end of the growing season in May and October.

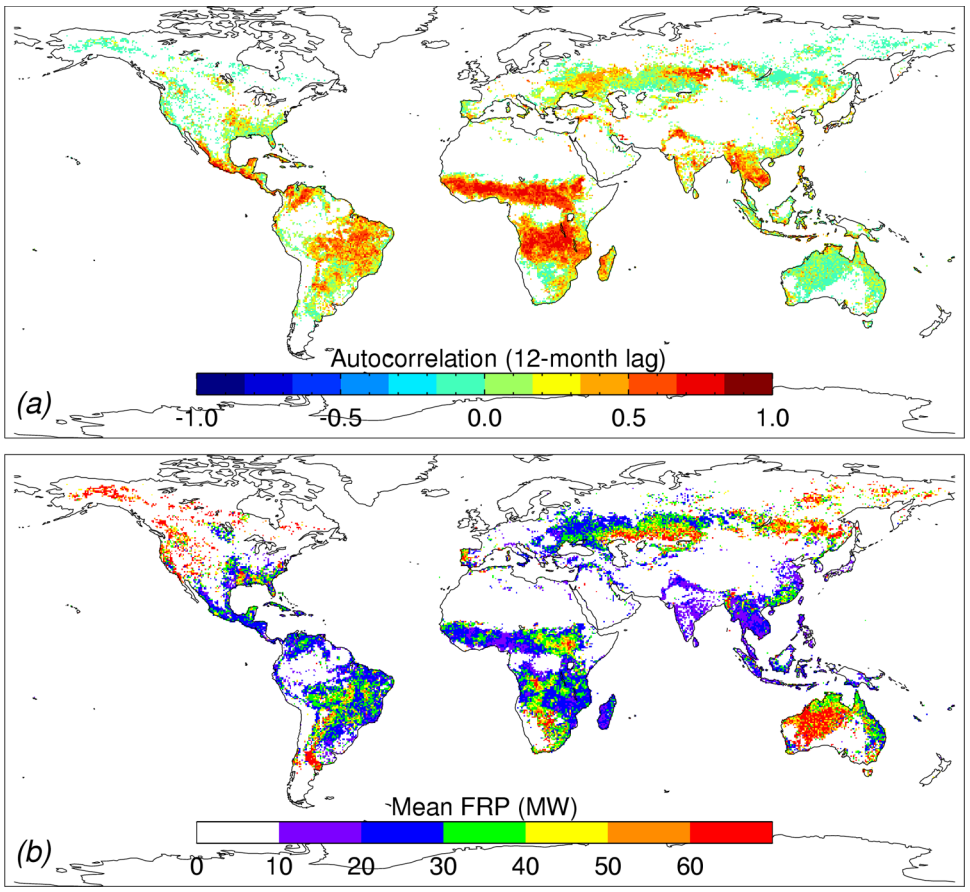

Figure 3. (a) Twelve-month lagged autocorrelation of the overpass-corrected fire count time series within each grid cell, and (b) mean annual fire radiative power (FRP).

[25] Regions of significant interannual variability (and significantly less periodicity) include the United States, southwest China, Siberia, Canada, and virtually the entire Australian continent, reflecting the much more sporadic nature of fire in these locations. In both Siberia and boreal North America large fires occur in areas of extensive forest cover, which require very long time periods for regrowth, making it unusual for a given patch of vegetation to burn in successive years.

4.3. Fire Radiative Power

[26] The climatological fire radiative power for the Terra MODIS is shown in Figure 3b. In general, low FRP (~15 MW) tends to be associated with areas of extensive cropland, regardless of location, reflecting the fact that agricultural fires are usually controlled and remain small. In the tropics and much of the subtropics, low FRP is also associated with more heavily forested areas, while higher FRP (~40 MW) tends to occur in grassland areas. In the absence of cutting trees and a subsequent drying period, fuel moisture in tropical forests is usually too high to permit large (or intense) fires; fires that do manage to burn are more likely to consist of cooler, smoldering combustion. Lighter herbaceous fuels, however, dry out much more quickly and are consumed via hotter flaming combustion. The hotter, flaming fires of the grasslands of northern and western Australia show the largest area of high FRP. These fires are more energetic than the savanna fires in Africa and Brazil. In boreal forests a very different trend is observed. Here very high FRP (~80 MW) occurs in areas having greater tree cover and less herbaceous vegetation, reflecting the very large fuel loads available in boreal forest.

[27] Several smaller-scale features stand out in the spatial distribution of the fire radiative power. First, the band of anomalously high FRP (~60 MW) in the Rio Negro Province of Argentina is confined to a relatively narrow swath of xeromorphic shrubland [*Soares*, 1990]. Second, the highest values of FRP (up to 600 MW) occur in the boreal zones of Siberia, Canada, and Alaska. In these regions, which are predominantly forested, dry-weather fuel loads are extremely high, and the size of the actively burning areas can grow to be very large. Higher radiative power is to be expected from the more energetic crown fires in these regions, and the FRP could potentially allow crown vs. surface fires to be distinguished remotely. *Wooster and Zhang* [2004] used MODIS FRP to demonstrate that North American boreal forest fires are dominated by crown fires, whereas Siberian forest fires are less intense and most likely burn at the surface. We found a 5-year mean FRP of 81.2 MW in boreal North America versus 53.7 MW in boreal Russia, a result consistent with their findings. Finally, the prominent latitudinal FRP gradient in Ukraine, Russia, and Kazakhstan very closely matches the land cover transition from cropland to grassland. This pattern is consistent with

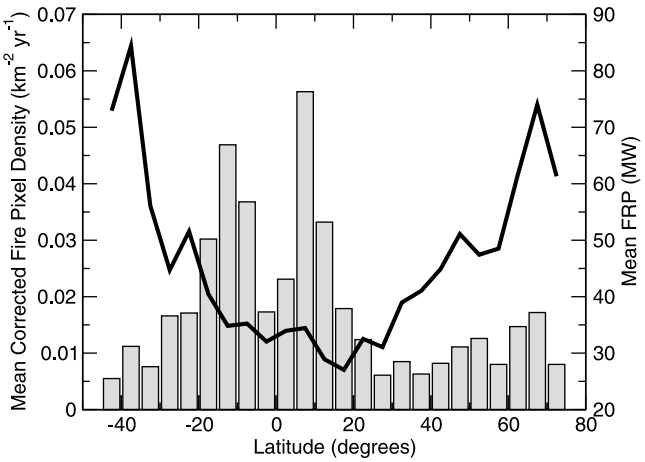

Figure 4. Mean density of overpass-corrected fire pixels (gray bars) and mean fire radiative power (black line) within 5° latitude zones from the first 5 years of Terra MODIS observations.

the corresponding latitudinal gradient in temporal autocorrelation seen in Figure 3a.

[28] The latitudinal distributions of mean fire pixel density and mean FRP in 5° zones are shown in Figure 4. The most notable feature is the general increase in FRP with increasing latitude, which is opposite the trend of higher fire pixel densities at lower latitudes on either side of the equator. Both trends are entirely consistent with the general decrease in temporal autocorrelation toward higher latitudes. Taken as a whole, the trends in all three quantities are indicative of a general shift from more-controlled seasonal burning in the tropics and subtropics (with lower fuel loads), to less-controlled episodic fires at higher latitudes (with higher fuel loads). A second feature evident in Figure 4 is the asymmetry of zonal FRP with respect to the equator. This asymmetry arises from the different distributions of land and fire regimes within the Northern and Southern Hemispheres, in particular the combination of the relatively low FRP contributed by India and Southeast Asia with the relatively high FRP contributed by Australia and Argentina.

4.4. Diurnal Fire Cycle

[29] The Terra and Aqua satellites lie in polar orbits with local equatorial crossing times of 1030/2230 and 0130/1330, respectively. This offers the opportunity to examine different points of the diurnal fire cycle. Previous work by *Prins and Menzel* [1992], *Eva and Lambin* [1998], *Pack et al.* [2000], *Justice et al.* [2002], and *Giglio et al.* [2003c] has shown that such a cycle exists in Africa, Brazil, and parts of Indonesia, but both the extent and magnitude of this cycle has yet to be established over most of the globe.

[30] A separate analysis (not shown) revealed that the majority (~90%) of Terra and Aqua MODIS fire pixels in the tropics and subtropics were detected during the daytime overpasses. Therefore a comparison of all (i.e., both daytime and nighttime) Terra MODIS fire pixels to all Aqua MODIS fire pixels primarily reflects a difference in the diurnal fire cycle between midmorning and early afternoon. To this end, we show the fraction of all (Terra + Aqua) overpass-corrected fire pixels detected by the Aqua MODIS instrument within each 0.5° grid cell in Figure 5. On the basis of this figure one may, to first order, divide the globe into three classes: (1) areas of negligible morning fire

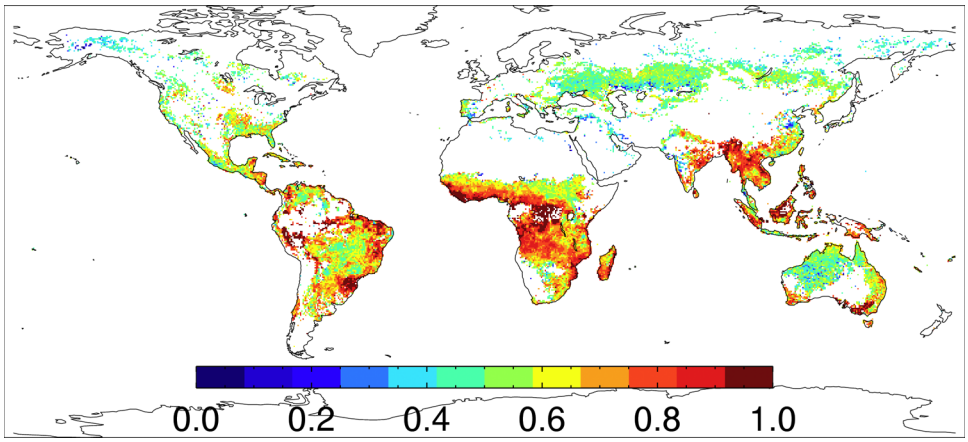

Figure 5. Ratio of overpass-corrected Aqua fire pixel counts to total (Aqua + Terra) overpass-corrected fire pixel counts from July 2002 through June 2005. Red and orange colors indicate regions in which a significant diurnal fire cycle exists.

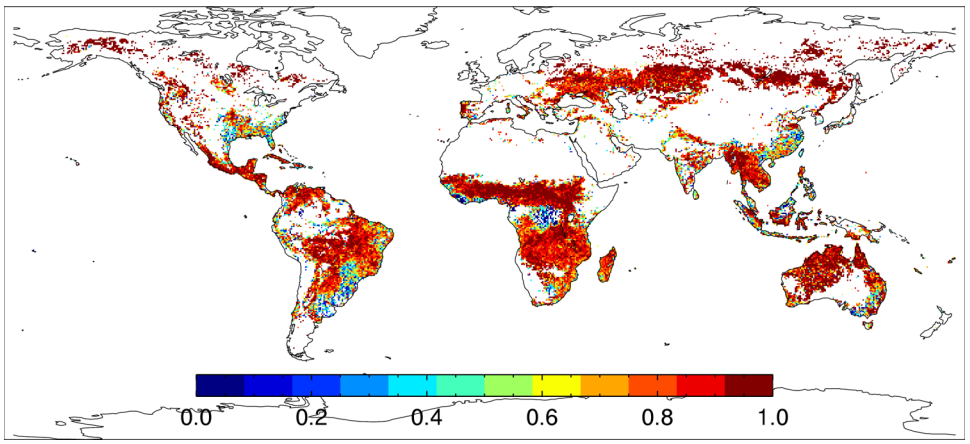

Figure 6. Cross correlation of Terra versus Aqua overpass-corrected monthly fire pixel counts from July 2002 to October 2005.

activity, with nearly 100% of all fire pixels detected by the Aqua MODIS; (2) areas of predominantly early afternoon fire activity, with about 75% of all fire pixels detected by the Aqua MODIS; and (3) areas where early afternoon and midmorning fire activity are about evenly matched. The first category tends to occur in the broadleaf forests of West Africa, Central Africa, Borneo, and Brazil, and cropland in southeast Australia. The second category occurs primarily in southern and sub-Saharan Africa (with notable exceptions in Sudan and Ethiopia), Southeast Asia, Indonesia, southwest Australian cropland, and a large crescent-shaped swath in eastern Brazil of comparatively heterogeneous vegetation cover. The final category is found primarily in northern and western Australia, central Eurasia, and the boreal forests of Siberia and North America. Within this last category are fires that, once ignited, typically burn for at least several days and up to many weeks.

[31] A complication that we have touched on in the previous discussion is that the MODIS instruments make multiple daytime and nighttime observations at high latitudes each day since the Terra and Aqua satellites reside in sun-synchronous polar orbits. This means that, at high latitudes, each instrument samples more than two local times (one daytime plus one nighttime) of the diurnal cycle each day. (The extreme case occurs at the poles with nearly 15 observations each day.) As a result, the local time windows sampled at boreal latitudes by each of the MODIS instruments overlap, and the ratio we show in Figure 5 is in fact not a consistent measure of the degree to which a diurnal fire cycle might exist. At boreal latitudes the simple fire-count ratio can potentially mute the apparent magnitude of the diurnal fire cycle owing to the overlap in local observation times. Nevertheless, Figure 5 does illustrate the minimum spatial extent of regions having a pronounced diurnal fire cycle.

5. Terra/Aqua MODIS Comparison

5.1. Time Series Comparison

[32] The previous analysis of the diurnal fire cycle raises the practical issue of the consistency of the fire time series recorded by the two MODIS instruments. Clearly there will be differences in the absolute numbers of fire pixels detected with each (see Figure 5), but of equal concern are potential differences in the seasonality of fire activity. To quantify the consistency in seasonality, we calculated the cross correlation of the Terra and Aqua overpass-corrected fire-pixel time series for each grid cell from July 2002 through October 2005 (Figure 6). The cross correlation is sensitive to differences in the timing of fire activity (fire season length, location and number of peaks), but relatively insensitive to differences in the magnitude of the time series.

[33] In general, the cross-correlation of the two time series was high (~0.9) in most areas of the world, indicating that the two MODIS instruments generally show good agreement with respect to the peak month of fire activity and the length of the fire season. Exceptions occur in the southeastern United States, eastern South America, Liberia, central Africa, eastern China, Borneo, and southeast Australia. To help understand these "anomalous" cases we examined the individual monthly time series in spatial windows located within each region (Table 1). Six examples are shown in Figures 7a–7f. For comparison, we also show the time series for four regions having a high cross correlation (Figures 7g–7j).

[34] The largest discrepancies in seasonality uniformly occurred in the tropical rain forests of Liberia, Borneo, Central Africa, and the Amazon Basin. Here, Aqua yields fire seasons 5 to 10 times longer than those derived from

Table 1. Regions Considered in Terra/Aqua time Series Comparison, With Cross-Correlation Coefficients for the Overlapping Portion of the Time Series (July 2002 to October 2005) Shown in Figure 6

Name	Latitude	Longitude	Cross Correlation
Southeast USA	27.5°N–33°N	84°W–80.5°W	0.77
Eastern Argentina	32°N–38.5°N	64°W–58.5°W	0.87
Liberia	4°N–7.5°N	11°W–7°W	0.26
Central Africa	3°S–1.5°N	20.5°E–29°E	0.61
Eastern China	28.5°N–32°N	116°E–122°E	0.62
Southeast Australia	34°S–38°S	140°E–145.5°E	0.54
Pacific Northwest USA	42°N–52°N	125°W–115°W	0.99
Southeast Russia	49°N–54°N	110°E–135°E	0.99
Southern Africa	6°S–14° S	15°E–30°E	0.98
Northern Australia	12°S–21°S	126°E–137°E	0.96

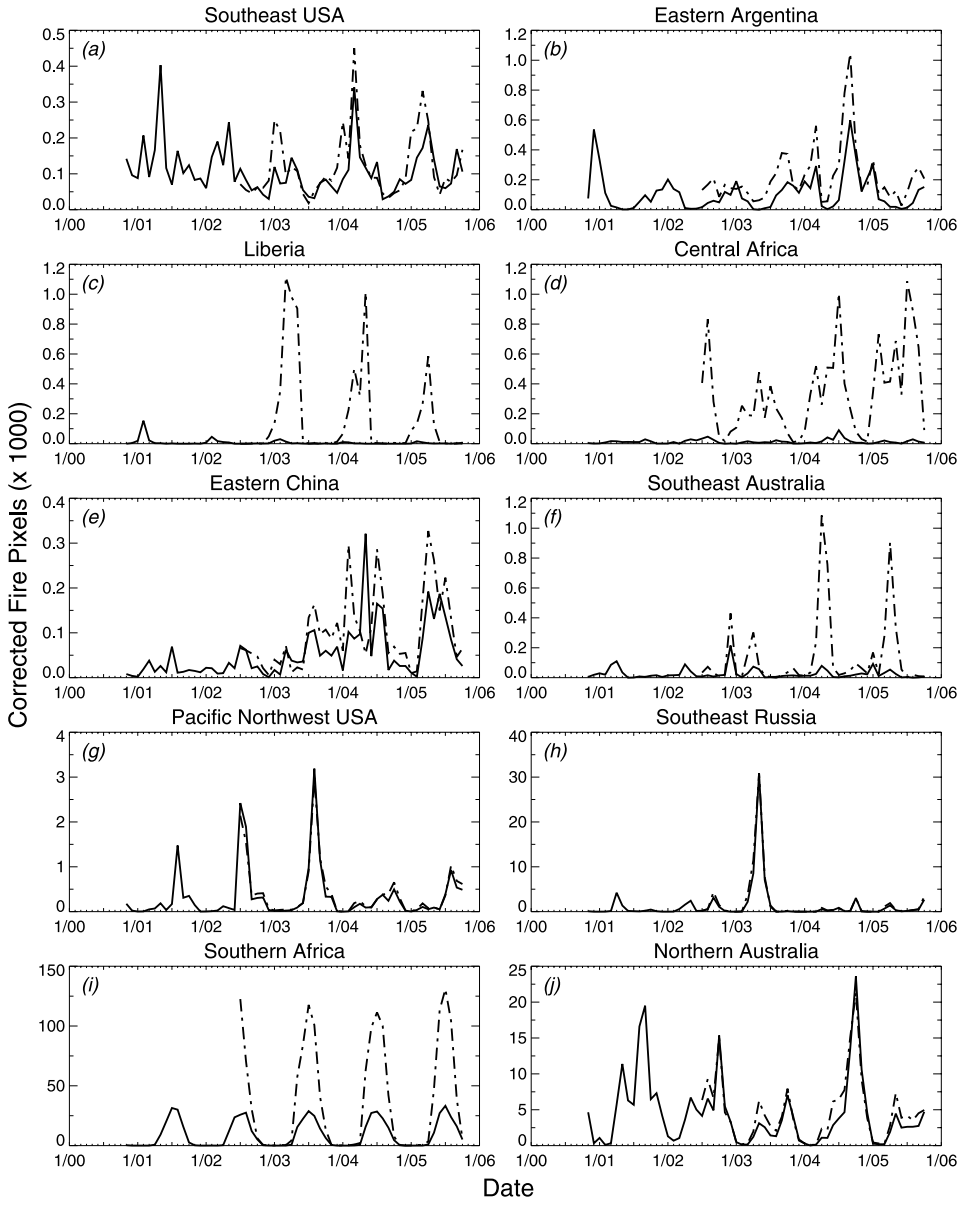

Figure 7. Time series of Terra (solid line) and Aqua (dashed line) overpass-corrected fire pixel counts for 10 different regions. (a–f) Regions in which the time series have a low cross-correlation. (g–j) Regions in which the time series have a very high cross-correlation. Geographic boundaries of the different regions are listed in Table 1. The horizontal axis spans the time period from January 2000 through January 2006 (1/00, January 2000; 1/01, January 2001; etc.).

Terra observations (Figures 7c and 7d). The time series as well as Figure 4 show that an extremely strong diurnal fire cycle exists in tropical rain forest, rendering the Terra MODIS virtually blind to fires in this ecosystem. To a slightly lesser extent this observation also applies to the dry forests of southeast Australia (Figure 7f). Southeast United States, eastern Argentina, and eastern China (Figures 7a, 7b, and 7e, respectively) are characterized by a relatively weak diurnal fire cycle and show some notable discrepancies in the months during which peaks occurred. In these regions, the poorer consistency of the Terra and Aqua time series likely stems from the more heterogeneous types of fires within each, including managed prescribed fires, burning of agricultural waste, and arson. Each fire category is likely to follow different seasonal and diurnal cycles. In combination, one would expect a less coherent time series that is not necessarily consistent between the two platforms.

[35] We note that the time series for southeast Australia, Pacific Northwest United States, and southeast Russia (Figures 7f–7h) illustrate the importance of using long-term time series to capture interannual variability in biomass burning. Climatologies based on 1 or 2 years of active fire observations can greatly misrepresent "normal" levels of fire activity over large areas of the globe. Indeed, nearly 40% of all fire-affected grid cells in our 5-year Terra MODIS fire climatology have a temporal autocorrelation (Figure 3a) less than 0.1 (i.e., these cells exhibit very significant interannual variability). We recognize that this

fraction does not include grid cells for which even a 5-year time series is insufficient to capture the episodic fires characteristic of some regions (e.g., boreal forest).

[36] In the above analysis, we have ascribed differences in the Terra and Aqua time series to the different sampling of the diurnal fire cycle, but there are at least two additional mechanisms by which differences can arise. First, the performance of the detection algorithm, both in terms of the probability of detecting a fire as well as the likelihood of yielding a false detection, is dependent upon environmental conditions that vary with respect to time of day, including surface temperature and solar zenith angle. Second, intrinsic differences in the Terra and Aqua MODIS instruments (or their calibration) could potentially contribute to a difference in observed fire activity.

[37] To estimate the magnitude of these effects relative to that of the diurnal fire cycle, we examined the fire time series in three different regions containing high-temperature sources that were not expected to show a significant diurnal cycle: the Kilauea volcano on the southernmost island of Hawaii, and gas flares associated with oil fields in southern Iraq and the Niger Delta. The July 2002 to December 2004 time series for each region is shown in Figure 8. For Kilauea and the Niger Delta, the magnitude of the discrepancies in the Terra and Aqua fire-pixel time series are well within the uncertainties entailed by cloud obscuration. In southern Iraq, Terra fire counts are consistently higher (≈16%) than those of Aqua. This is most likely caused by the near-infrared minimum-reflectance test used in the detection algorithm, which is preventing detection of some gas flares at the time of the Aqua overpass when the top-of-atmosphere reflectance is slightly higher. While a 16% discrepancy is not negligible, this case probably illustrates the effect at its largest owing to the abundance of bright soil in this region.

5.2. FRP Comparison

[38] We also compared the July 2002 to October 2005 global distribution of mean FRP derived from Aqua observations with that derived from Terra observations for the same time period. The Aqua FRP distribution was very similar to that of Terra, but approximately 10% larger in magnitude. This difference may be explained by Aqua's afternoon sampling of the diurnal fire cycle, at which time fires tend to be burning in larger numbers and with greater intensity.

6. Impact of Cloud Correction

[39] As mentioned in section 2.1, the additional cloud correction applied to the overpass-corrected monthly fire pixel counts is based on the assumption that the number of fire pixels per unit area within both clear and cloud-obscured areas is identical. Beneath raining clouds this assumption is unreasonable, and the correction in (3) is likely to overestimate the true extent of fire activity. In the absence of a correction for variable cloud cover, however, the monthly fire-count time series could potentially contain significant artificial drops during periods of increased cloudiness. To test the sensitivity of the results in sections 4 and 5 to variations in cloud cover, we repeated our analyses with overpass-corrected fire-pixel counts containing the additional cloud correction (i.e., N''_{fire} versus N'_{fire}). At the 0.5° monthly spatial and temporal scales used in this study, we found no significant differences in fire seasonality (peak month and season length) following application of the cloud correction. While the correction did noticeably increase the absolute number of fire pixels in each grid cell (by about 20%), the relative distribution of fire activity was essentially unchanged.

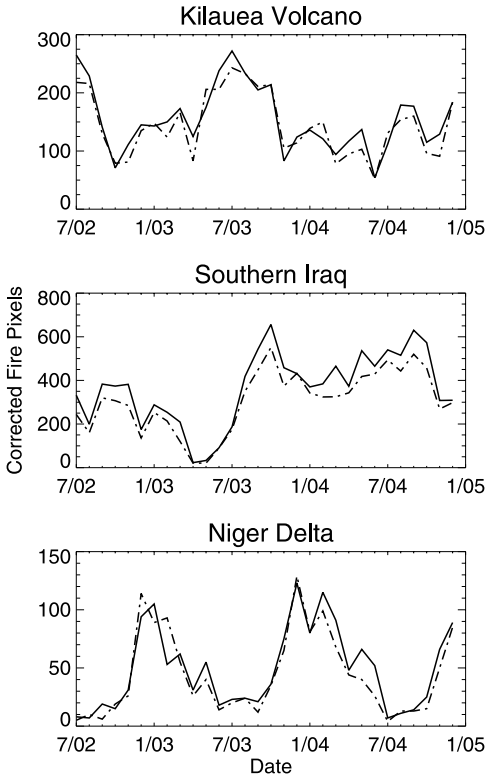

Figure 8. July 2002 to October 2005 time series of Terra (solid line) and Aqua (dashed line) overpass-corrected fire pixel counts for three different regions containing persistent, non-vegetation-fire hot spots. (top) Kilauea volcano, Hawaii (∼19.4°N, 155.1°W). (middle) Gas flares in southern Iraq (approx. 30.5°N, 47.4°E). (bottom) Gas flares in oil fields of the Niger Delta, Nigeria (∼4.8°N, 5.7°E). (Note that the time series shown here are shorter than those in Figure 6. This is because we used a slightly older version of the CMG product, which did not have persistent hot spots removed, for this part of the analysis. The overpass-corrected fire pixel counts were otherwise identical.)

7. Conclusion

[40] In this study we have used the 0.5° monthly Terra MODIS CMG fire product from November 2000 through October 2005 to analyze the global distribution of biomass burning. Using these data, we derived five different metrics characterizing different aspects of large-scale fire behavior. Among these metrics we considered the mean fire radiative power (FRP) for the first time at a global scale. Low FRP was associated with areas of extensive cropland regardless of location. In the tropics and much of the subtropics, low FRP was also associated with more heavily forested areas,

while higher FRP was associated with areas having more herbaceous vegetation. In boreal regions this trend was reversed, with higher FRP occurring in areas having more tree cover and less herbaceous vegetation. Although not explored in the present work, the FRP is an important potential link to producing pyrogenic emissions estimates.

[41] At the global scale, July, August, and September are the peak months of fire occurrence, with fires in both the northern and southern hemispheres, while February is least often the month of peak fire occurrence. For every month, there is fire activity somewhere on the planet.

[42] Globally, the duration of the annual fire season usually varies between 2 and 6 months and is, in the tropics, highly constrained by the duration of the dry season. Exceptionally long fire seasons of $\sim$10 months occur in central and southern Brazil and the southeastern United States. The duration of the fire season at boreal latitudes is uniformly short at 1–3 months.

[43] The lowest interannual variability, as indicated by the highest 12-month lagged temporal autocorrelation, was observed in the savannas of Africa, both in the Sudanian and Sahelian zones north of the equator and in central and southern Africa between 5°S and 20°S. This characteristically strong annual periodicity is caused by a combination of widespread human-induced burning for land maintenance purposes and low interannual variability in rainfall during the study period. Regions of significant interannual variability (and significantly less periodicity) include the United States, southwest China, Siberia, Canada, and most of Australia.

[44] By combining 3 years of Terra and Aqua MODIS observations we were able to identify regions having a pronounced diurnal fire cycle. We found that this cycle is extremely strong, at least between the midmorning and early afternoon Terra and Aqua overpass, in the broadleaf forests of West Africa, Central Africa, Borneo, and Brazil, and cropland in southeast Australia. In these regions virtually all fires are detected exclusively during the afternoon Aqua overpass. The diurnal fire cycle was weaker but still significant in southern and sub-Saharan Africa (with exceptions in Sudan and Ethiopia), Southeast Asia, Indonesia, and parts of southwest Australia and Brazil. The cycle appears to be insignificant in northern and western Australia, central Eurasia, and the boreal forests of Siberia and North America, but of course we have sampled only a few points on a curve that might change substantially between satellite overpasses. Further work with data from the VIRS, on board the precessing TRMM satellite, and the newer generation of geostationary satellites is desirable to more fully understand this cycle. Implicit in any approach using satellite data is the need for a better understanding of the fire monitoring capabilities of specific sensors which result from the physical characteristics of the sensor itself, the fire detection (and characterization) algorithms used with each sensor, and the orbital characteristics of the satellite platform on which the sensor resides.

[45] We examined the consistency of the fire time series recorded by the Terra and Aqua MODIS instruments and found that, in most areas, the month of peak burning and fire season length observed by each were in good agreement. The largest discrepancies in seasonality uniformly occurred in tropical rain forests, and are the result of an extremely strong diurnal fire cycle that exists in this ecosystem.

[46] The individual spatial and temporal metrics used in our analysis quantify different aspects of fire behavior at the global scale. Together they can be used to quantitatively monitor changes in fire behavior at a global scale. Additional insight could potentially be afforded by combining these metrics into unique classes of distinct fire characteristics. In many respects, the set of such classes would be the ''satellite analog'' of the ecological concept of fire regime, a semiquantitative summary of fire seasonality, fire type (e.g., surface, crown), and fire return interval [*Whelan*, 1995]. The satellite data record, in this case 5 years, is clearly too short to address the full range of global fire return intervals. A more pragmatic application of such a classification would be to stratify the land surface into regions of homogeneous fire behavior, and thus simplify the parameterization of fire-related variables in global emissions, transport, and biogeophysical models [e.g., *Streets et al.*, 2003; *Arellano et al.*, 2004]. Earlier attempts to identify satellite-based fire regimes have been made by *Dwyer et al.* [1999] and *Clerici et al.* [2004] using comparatively short records ($\leq$1 year) of fires observations. Future work with the full MODIS time series, including the fire radiative power, should contribute to these efforts.

[47] While the MODIS CMG fire product provides useful information about the spatial and temporal dynamics of global fire activity, the distribution of fire activity within different land cover types, and fire intensity (via the FRP), it is important to keep the inherent limitations of this data set in mind. First, the fundamental unit of observation, the ''fire pixel,'' does not necessarily correspond to a single fire, but indicates instead that one or more fires, or portions of larger fires, are contained within the pixel at the time of the satellite overpass. Second, the data set captures only a subset of fires since not every fire is detected, generally because of limitations in the instrument and detection algorithm, obscuration by clouds, or the limited diurnal sampling afforded by the satellite orbit. Third, the number of fire pixels observed within a grid cell is not necessarily indicative of the total area burned within the grid cell. While it is not uncommon to assume that burned area is proportional to counts of fire pixels, this can lead to unreliable estimates of burned area [*Eva and Lambin*, 1998; *Kasischke et al.*, 2003]. Use of additional fire-pixel clustering information and ancillary vegetation data can, however, improve the quality of such estimates [*Giglio et al.*, 2006].

[48] **Acknowledgment.** We thank James Randerson, Eric Kasischke, and an anonymous reviewer for helpful technical suggestions.

References

Abram, N. J., M. K. Gagan, M. T. McCulloch, J. Chappell, and W. S. Hantoro (2003), Coral reef death during the 1997 Indian ocean dipole linked to Indonesian wildfires, *Science*, *301*, 952–955.

Andreae, M. O. (1991), Biomass burning: Its history, use, and distribution and its impact on environmental quality and global climate, in *Global Biomass Burning*, edited by J. S. Levine, pp. 3–21, MIT Press, Cambridge, Mass.

Arellano, A. F., Jr., P. S. Kasibhatla, L. Giglio, G. R. van der Werf, and J. T. Randerson (2004), Top-down estimates of global CO sources using MOPITT measurements, *Geophys. Res. Lett.*, *31*, L01104, doi:10.1029/2003GL018609.

Arino, O., and J. Rosaz (1999), 1997 and 1998 world ATSR fire atlas using ERS-2 ATSR-2 data, in *Proceedings of the Joint Fire Science Confer-*

ence, edited by L. F. Neuenschwander, K. C. Ryan, and G. E. Golberg, pp. 177–182, Univ. of Idaho, Boise.

Clerici, N., L. Boschetti, H. Eva, and J.-M. Grégoire (2004), Assessing vegetation fires activity and its drivers in west-central Africa using MODIS and TRMM data, paper presented at International Geoscience Remote Sensing Symposium, IEEE Comput. Soc., Piscataway, N. J.

Csiszar, I., L. Denis, L. Giglio, C. O. Justice, and J. Hewson (2005), Global fire distribution from MODIS, *Int. J. Wildland Fire*, *14*, 117–130.

Dwyer, E., J. M. C. Pereira, J.-M. Grégoire, and C. C. DaCamara (1999), Characterization of the spatio-temporal patterns of global fire activity using satellite imagery for the period April 1992 to March 1993, *J. Biogeogr.*, *27*, 57–69.

Dwyer, E., J.-M. Grégoire, and J. M. C. Pereira (2000a), Climate and vegetation as driving factors in global fire activity, in *Biomass Burning and its Inter-Relationships with the Climate System*, edited by J. L. Innes, M. Beniston, and M. M. Verstraete, pp. 171–191, Springer, New York.

Dwyer, E., S. Pinnock, and J.-M. Grégoire (2000b), Global spatial and temporal distribution of vegetation fires as determined from satellite observations, *Int. J. Remote Sens.*, *21*, 1289–1302.

Edwards, D. P., et al. (2004), Observations of carbon monoxide and aerosols from the Terra satellite: Northern Hemisphere variability, *J. Geophys. Res.*, *109*, D24202, doi:10.1029/2004JD004727.

Edwards, D. P., et al. (2005), Satellite-observed pollution from Southern Hemisphere biomass burning, *J. Geophys. Res.*, doi:10.1029/2005JD006655, in press.

Elvidge, C. D., K. E. Baugh, E. A. Kihn, H. W. Kroehl, and E. R. Davis (1997), Mapping city lights with nighttime data from the DMSP Operational Linescan System, *Photogramm. Eng. Remote Sens.*, *63*, 727–734.

Eva, H., and E. F. Lambin (1998), Remote sensing of biomass burning in tropical regions: Sampling issues and multisensor approach, *Remote Sens. Environ.*, *64*, 292–315.

Giglio, L., J. D. Kendall, and C. O. Justice (1999), Evaluation of global fire detection algorithms using simulated AVHRR infrared data, *Int. J. Remote Sens.*, *20*, 1947–1985.

Giglio, L., J. D. Kendall, and R. Mack (2003a), A multi-year active fire data set for the tropics derived from the TRMM VIRS, *Int. J. Remote Sens.*, *24*, 4505–4525.

Giglio, L., J. Descloitres, C. O. Justice, and Y. Kaufman (2003b), An enhanced contextual fire detection algorithm for MODIS, *Remote Sens. Environ.*, *87*, 273–282.

Giglio, L., J. Pinzon, and P. Kasibhatla (2003c), Comment on "Seasonal, intraseasonal, and interannual variability of global land fires and their effects on atmospheric aerosol distribution" by Y. Ji and E. Stocker, *J. Geophys. Res.*, *108*(D24), 4754, doi:10.1029/2003JD003548.

Giglio, L., G. R. van der Werf, J. T. Randerson, G. J. Collatz, and P. Kasibhatla (2006), Global estimation of burned area using MODIS active fire observations, *Atmos. Chem. Phys.*, *6*, 957–974.

Hansen, M. C., R. S. DeFries, J. R. G. Townshend, M. Carroll, C. Dimiceli, and R. A. Sohlberg (2003), Global percent tree cover at a spatial resolution of 500 meters: First results of the MODIS vegetation continuous fields algorithm, *Earth Interact.*, *7*(10), doi:10.1175/1087-3562.

Ichoku, C., Y. Kaufman, L. Giglio, Z. Li, R. H. Fraser, J.-Z. Jin, and W. M. Park (2003), Comparative analysis of daytime fire detection algorithms using AVHRR data for the 1995 fire season in Canada: Perspective for MODIS, *Int. J. Remote Sens.*, *24*, 1669–1690.

Johnson, E. A. (1992), *Fire and Vegetation Dynamics: Studies From the North American Boreal Forest*, Cambridge Univ. Press, New York.

Justice, C. O., and S. Korontzi (2001), A review of the status of satellite fire monitoring and the requirements for global environmental change research, in *Global and Regional Wildfire Monitoring from Space: Planning a Coordinated International Effort*, edited by F. J. Ahern, J. Goldammer, and C. O. Justice, pp. 1–18, SPB Acad., Hague, Netherlands.

Justice, C. O., L. Giglio, S. Korontzi, J. Owens, J. Morisette, D. Roy, J. Descloitres, S. Alleaume, F. Petitcolin, and Y. Kaufman (2002), The MODIS fire products, *Remote Sens. Environ.*, *83*, 244–262.

Kasischke, E. S., N. L. Christensen Jr., and B. J. Stocks (1995), Fire, global warming and the mass balance of carbon in boreal forests, *Ecol. Appl.*, *5*, 437–451.

Kasischke, E. S., J. H. Hewson, B. Stocks, G. van der Werf, and J. Randerson (2003), The use of ATSR active fire counts for estimating relative patterns of biomass burning: A study from the boreal forest region, *Geophys. Res. Lett.*, *30*(18), 1969, doi:10.1029/2003GL017859.

Kaufman, Y. J., C. O. Justice, L. P. Flynn, J. D. Kendall, E. M. Prins, L. Giglio, D. E. Ward, W. P. Menzel, and A. W. Setzer (1998), Potential global fire monitoring from EOS-MODIS, *J. Geophys. Res.*, *103*(D24), 32,315–32,338.

Kaufman, Y., C. Ichoku, L. Giglio, S. Korontzi, D. A. Chu, W. M. Hao, R.-R. Li, and C. O. Justice (2003), Fires and smoke observed from the Earth Observing System MODIS instrument—Products, validation, and operational use, *Int. J. Remote Sens.*, *24*, 1765–1781.

Pack, D. W., C. J. Rice, B. J. Tressel, C. J. Lee-Wagner, and E. M. Oshika (2000), Civilian uses of surveillance satellites, *Crosslink*, *1*(1), 2–8.

Prins, E. M., and W. P. Menzel (1992), Geostationary satellite detection of biomass burning in South America, *Int. J. Remote Sens.*, *13*, 2783–2799.

Ramankutty, N., and J. A. Foley (1998), Characterizing patterns of global land use: An analysis of global croplands data, *Global Biogeochem. Cycles*, *12*, 667–685.

Rosenfeld, D. (1999), TRMM observed first direct evidence of smoke from forest fires inhibiting rainfall, *Geophys. Res. Lett.*, *26*, 3105–3108.

Scottish Environment Protection Agency (SEPA) (2002), *Guidance on Landfill Gas Flaring*, Environ. Agency, Bristol, U.K.

Soares, R. V. (1990), Fire in some tropical and subtropical South American vegetation types: An overview, in *Fire in the Tropical Biota*, edited by J. G. Goldammer, pp. 63–81, Springer, New York.

Streets, D. G., K. F. Yarber, J.-H. Woo, and G. R. Carmichael (2003), Biomass burning in Asia: Annual and seasonal estimates and atmospheric emissions, *Global Biogeochem. Cycles*, *17*(4), 1099, doi:10.1029/2003GB002040.

Stroppiana, D., S. Pinnock, and J.-M. Grégoire (2000), The Global Fire Product: Daily fire occurrence from April 1992 to December 1993 derived from NOAA AVHRR data, *Int. J. Remote Sens.*, *21*, 1279–1288.

van der Werf, G. R., J. T. Randerson, G. J. Collatz, and L. Giglio (2003), Carbon emissions from fires in tropical and subtropical ecosystems, *Global Change Biol.*, *9*, 547–562.

Weber, M. G., and M. D. Flannigan (1997), Canadian boreal forest ecosystem structure and function in a changing climate: Impact on fire regimes, *Environ. Rev.*, *5*, 145–166.

Whelan, R. J. (1995), *The Ecology of Fire*, Cambridge Univ. Press, New York.

Wooster, M. J., and Y. H. Zhang (2004), Boreal forest fires burn less intensely in Russia than in North America, *Geophys. Res. Lett.*, *31*, L20505, doi:10.1029/2004GL020805.

Wooster, M. J., B. Zhukov, and D. Oertel (2003), Fire radiative energy for quantitative study of biomass burning: Derivation from the BIRD experimental satellite and comparison to MODIS fire products, *Remote Sens. Environ.*, *86*, 83–107.

I. Csiszar and C. O. Justice, Department of Geography, University of Maryland at College Park, College Park, MD 20742, USA.

L. Giglio, NASA Goddard Space Flight Center, Code 614.4, Greenbelt, MD 20771, USA. (giglio@hades.gsfc.nasa.gov)